International Journal of Engineering Works
ISSN-p: 2521-2419
ISSN-e: 2409-2770
Vol. 5, Issue 9, PP. 138-146, September 2018
https://www.ijew.io/

An Investigation on the Flow Behavior in the Airfoil of a Flapping Wing

M.Amin Nikbakht[1], Soheil Mohtaram[2], Mohammad Hasan Moghadas[3]
Department of Mechanical Engineering, Islamic Azad University, Esfahan, Iran, Amin.nikbakht88@gmail.com[1]
College of Mechanics and Materials, Hohai University, Nanjing 210098, China, Soheil@hhu.edu.cn[2]
Department of Mechanical Engineering, Malek-Ashtar University of Technology, Iran. mhmogh@yahoo.com[3]
Received: 21 July, Revised: 28 August, Accepted: 30 August

Abstract—In this investigation, the two-dimensional dynamic analyses of the wing airfoil of a swing-wing micro air vehicle (MAV) were carried under restrained pitching and flapping oscillations, which varied in the 10-degree oscillation range and the 0.1-10 reduced frequency range. The flow was in a laminar flow with a Reynolds number of 1100. The objective of this simulation was to study the flow behavior in the dynamic motions in a dynamic stall regime. Similar studies on the dynamic stall regime with low Reynolds numbers have not resulted in a particular numerical solution and have separately studied the parameters influencing the numerical solution. The most critical dynamic motions that require utmost precision in numerical analyses were reviewed and validated in this research. The results of the numerical research analyses were compared to the experimental results obtained with a water tunnel.

Keywords— micro air vehicle, flapping, pitching, dynamic stall, hysteresis

I. Introduction

Unmanned aerial vehicles (UAVs), which use for different purposes such as detection [1], and discovery [2], are among the most military equipment which commonly used by state armies. The lack of need for human pilots in these vehicles along with their size, weight, and low cost has increased the reliability of these vehicles as compared to other alternatives. Recently, UAVs are widely used and are classified into the military and nonmilitary categories by application [3]. Some of the military areas of application of UAVs include espionage and suicidal operations, and the increased reduction in the size of these vehicles is aimed at conducting intelligence operations and attaining military group goals. In addition to the mentioned military uses, these vehicles offer numerous capabilities in the sea, space and on land. Some of these applications include forestry, environmental protection, examination of petroleum and gas lines, etc. Nowadays, unmanned air vehicles are available in different forms and vary by weight and size. These vehicles are grouped into the unmanned air vehicle (UAV) and complex air vehicle (CAV) categories.

The first inclusive research on MAVs was conducted in 1993 by the RAND institute [4]. Later on, extensive research was carried out on micro air vehicles by various researchers [5]. Today, studies and activities are focused on the construction of MAVs smaller than 15cm for detection and rescue purposes [6]. These air vehicles are small in size and fly slowly [7]. MAVs are grouped into the categories of fixed-wing MAVs, rotary-wing MAVs, VTOL (vertical take-off and landing) micro air vehicles, and the so-called ornithopters. Currently, the design of most ornithopters is inspired by bird and insect anatomies [8]. The first functional ornithopter was built in 1870 in France. The Gustav Tropez flew about 70 meters in an exhibition held by the Académie des Sciences. The wings moved with the activation of the Bourdon tube by gunpowder. In 1871, Jobert et al. [9,10] used rubber bands to enable a small ornithopter to fly. Research on ornithopters has indicated that they are less common than fixed- and rotary-wing MAVs mainly because of their aerodynamic complexity. Hence, fewer studies have been conducted on fixed- and rotary-wing air vehicles [11]. Most micro air vehicle development works are focused on insect models. In spite of the challenges associated with the imitation of the complicated unsteady aerodynamic mechanisms of flapping wings with low Reynolds numbers, insects are considered valuable models in the design of MAVs due to advantages such as their small sizes and power-to-weight ratios. Ornithopter MAVs are generally classified into the NAV, PAV, and MAV groups. The design of MAV, PAV (Pico Air Vehicle), and NAV (Nano Air Vehicle) ornithopters are inspired by birds, insects, and bird-like insects, respectively. In the construction of ornithopter MAVs, shape memory alloys, piezoelectric materials and smart materials are used as flapping stimuli especially in the products of the NAV and PAV categories depending on weight. These materials are also commonly used in PAV micro air vehicles which aren't allow to be used in electric motors. Since bigger birds are unable to move their wings back and forth, they spread their wings downward along the strike direction. They bend their wings along the upward strike to reduce the drag. In general, bending is more highlighted during slow forward flying than rapid forward flying. This state of suspension in the asymmetric space is called the "bird strike" [12,13]. To avoid large drag forces and negative lift forces, these birds bend their wings upward along the strike direction by moving the primary feathers to allow for the inflow of air. Therefore, the dynamic motions of bird wings include simultaneous pitching (rotary movements) and plunging (upward and downward movements)

that together form the flapping function. These motions induce thrusting along the movement direction using the flow properties in the dynamic stall regime. The effects of the unsteadiness of flow were for the first time observed through the rapid variation of the attack angle of an airfoil by Kramer [14]. Following his preliminary research, the dynamic stall phenomenon attracted little attention due to the limited precision of the data collection equipment of the time until extensive research was conducted on the adverse effects of the dynamic stall in 1960 [15,16]. This attention was the result of the abrupt deviation of the pitching moment from the static state, the resulting constraints on the flight coverage of air vehicles, and the need for selection of materials for helicopter propellers. Dynamic stall has also been observed in the propellers of wind turbines [17, 19]. This phenomenon limits the performance of turbines and results in the structural fatigue of the propellers [20]. The result of these consequences is the increase in the overhaul and maintenance costs. In the wind turbine propellers, the dynamic stall is mainly the result of the unsteady inflow, abrupt winds, and rapid wind direction variations [21, 22]. In fixed-wing air vehicles, the flow of a large volume of flow perpendicular to the wing may cause the dynamic stall on the wing during the flight and irritate the occupants. One of the motives for the research on dynamic stall is the interest in omitting or reducing the damaging effects of this phenomenon [23-29]. However, it must be stated that this phenomenon is not always destructive and studies have been carried out on the utilization and control of this phenomenon in increasing the lift. This area of application is mainly considered in studying the flying behavior of insects and birds. Birds, insects, and fish generally move by flapping [30, 31]. Studies of birds suggest that the wing surface and its apparent ratio (AR) [32] are smaller than the body, which accounts for their steady flight [33]. Hence, the insects and birds utilize dynamic stall and increase the unsteady lift to remain suspended during the flight [34]. The need for increasing the maneuverability of aircraft has attracted the attention of researchers to airfoil pitching oscillations at large attack angles [35-37]. Moreover, the use of micro air vehicles for the military purposes and filming hard-to-reach places has been the motive of many researchers for studying and understanding the unsteady aerodynamics of dynamic stall and for increasing the lift force. In spite of all of the recent attempts and progress in understanding the separation of unsteady flows, the dynamic stall phenomenon is one of the major unsolved aerodynamic problems. Hence, a more precise understanding of flow separation is required for utilizing flows. On the other hand, it is impossible to carry out these examinations experimentally in a wind tunnel because of its high expenses and the numerical solution that gives a more precise understanding of flow separation is still unknown. Therefore, this study was an attempt to assess and validate numerical methods in the fluent commercial software.

In this research, a three-dimensional mesh was created using the square element method. Then, A C-type mesh was made, and the solution range covered a length 20 times the airfoil mid-chord in the flow upstream to a distance 30 times the airfoil mid-chord in the flow downstream. It also covered a diameter 20 times greater than the airfoil mid-chord in the upward and downward directions. The most straightforward and most practical method for the numerical simulation of a viscous flow involves the Navier–Stokes equations. The three-dimensional and incompressible Navier–Stokes equations were used in this research. Moreover, a computation method based on the control volume was used to solve the applicable equations.

II. The Nature Unsteady Flow on a Pitching Airfoil

For a more precise aerodynamic examination of a pitching model, a pitching airfoil is analyzed in this section. The results of this analysis, which are presented in the following, reflect the aerodynamic complexity of this airfoil. During the pitching of an airfoil (which occurs around one-quarter of its mid-chord), if the pitching occurs at the angles near the static stall, the lift hysteresis ring and pitching moment will be as shown in Figure. 2. Analyses of unsteady flows and phenomenon occurring during oscillations clarify the nature of flow on lambda wings. During pitching, when the attack angle of the oscillation model is larger than the stall attack angle in the static state (point a), first the reversal of flow in the boundary layer occurs and large eddies form in the boundary layer. As the attack angle grows, an eddy forms near the leading edge. The formation of the latter eddy increases the lift slope, which corresponds to point b. Meanwhile, the pitching moment stalls and the leading-edge eddy grows in size with an increase in the attack angle and moves toward the airfoil trailing edge until the dynamic lift factor is maximized and the airfoil stall begins. The result is the most harmful pitching moment. Following the full stall, as the attack angle decreases, the boundary layer is attached from the front of the airfoil to the rear and the surface of the airfoil (part d of the figure). When the flow connects to the surface, it returns to the static state.

The control of the dynamic stall eddy on the upper surface, which is aimed to delay its reattachment to the upper surface, increases the lift and transfers the dynamic stall angle for a long time during the pitching cycle to large attack angles [38]. The increase in the lift and delay of the dynamic stall attack angle depend on numerous parameters such as the oscillation range and frequency, flow regime, and Reynolds number [39, 40].

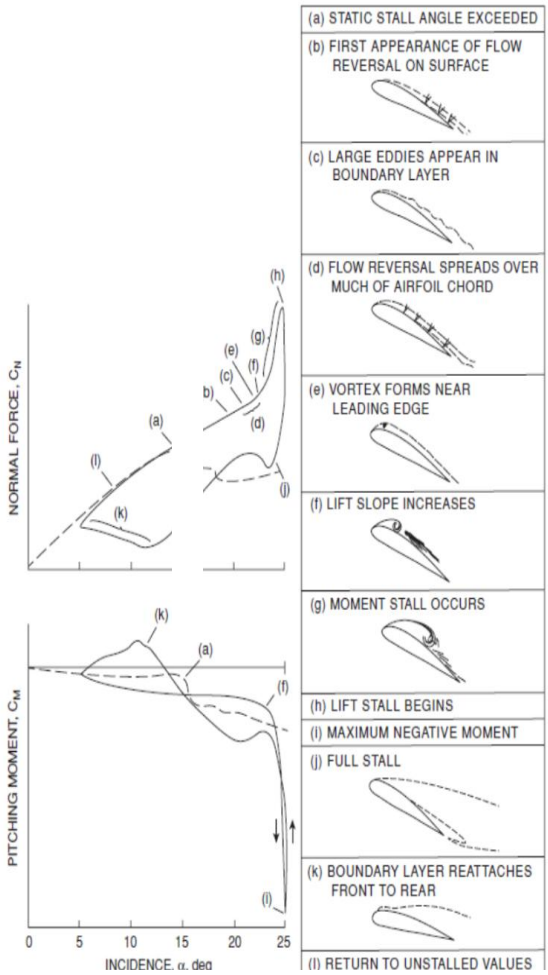

Figure.1. the dynamic stall phenomenon on a pitching airfoil [41]

I. 3. Mesh Generation and Numerical Solution Range

A. 3.1 Mesh Generation

In this research, a three-dimensional mesh was created using the square element method in ANSYS. A C-type mesh was generated, and the solution range covered a length 20 times the airfoil mid-chord in the flow upstream to a length 30 times the airfoil mid-chord in the flow downstream. It also covered a distance 20 times the airfoil mid-chord in the upward and downward directions (Fig. 2). The most straightforward and most practical method for the numerical simulation of a viscous flow involves the Navier–Stokes equations. The three-dimensional and incompressible Navier–Stokes equations were used in this research. Moreover, a computation method based on the control volume was used to solve the applicable equations.

The first step in the numerical simulation of flow in a field (especially in the presence of viscous flows) is meshing the field and converting it from a continuum into a discrete space for the application of numerical methods. It was tried to generate several 18000- to 91000-element meshes before the calculations and to numerically solve the problem under the conditions described in the following to select the optimum mesh for the subsequent analyses. To examine the effect of independence from the mesh, the number of nodes was increased as long as the drag coefficient remained unchanged and with the minimum difference from the experimental drag coefficient. Finally, a 43000-element mesh was used, and 20 rows of boundary layer elements were used on the airfoil. The first element height was 0.5mm. The mesh geometry is depicted in Fig. 4.

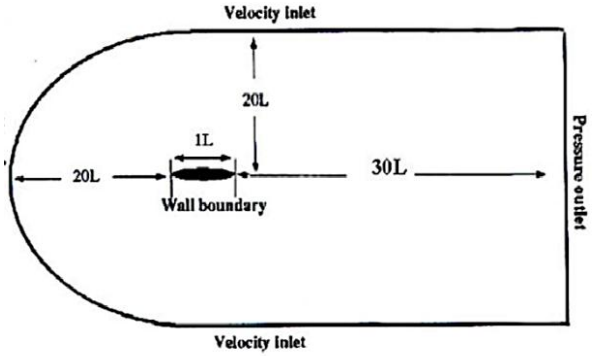

Figure.2. The computation range of the ornithopter airfoil

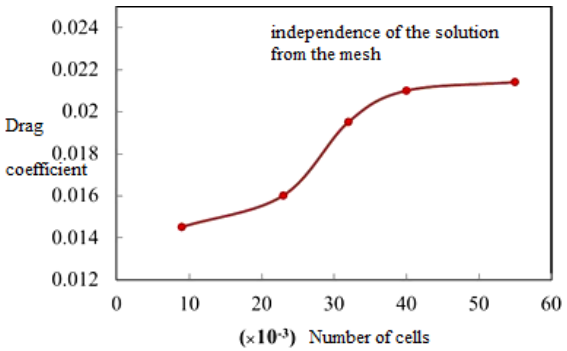

Figure.3. The effect of the independence of the solution from the mesh based on the drag coefficient

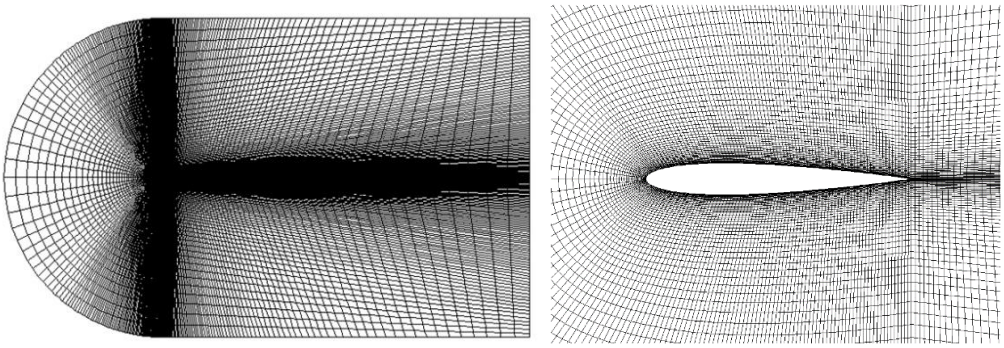

Figure.4. Organized elements around the NACA 0012 airfoil

B. 3.2 Numerical Simulation Method

The flow around the NACA 0012 airfoil was solved under sea level conditions. The inflow velocity was adjusted to have a Reynolds number of 1100. The pressure-based solver [42, 43] was used in the numerical analysis and the flow was solved as an unsteady flow. The coupling of velocity and pressure was used along with the second-order spatial discretization. The no-slip wall was used as the boundary condition for the airfoil and the boundary condition around the solution field was far-field pressure. The time step for the unsteady flow solution was 0.001.

1) 3.2.1 Main Dynamic Stall Parameters

One of the leading causes of the higher difficulty of the dynamic stall modeling and analysis as compared to static and steady stall modeling and analysis is the dependence of the former on several parameters. In the steady static state, the airfoil geometry, surface roughness, free flow turbulence, the Reynolds number, and Mach number influence the stall behavior [44]. However, during the dynamic oscillation of an airfoil at a constant pitching rate, stall depends on several parameters such as compressibility, Reynolds number, reduced oscillation frequency, oscillation axis position, three-dimensional flow, wind tunnel wall effects, and airfoil geometry. In addition, during sinusoidal airfoil oscillations, the maximum attack angle and the average attack angle are two of the critical parameters [45]. Numerical analyses have been carried out at small attack angles and reduced low frequencies, and given the low complexity of flow, it is possible to carry out these analyses using the most straightforward models and numerical algorithms with relatively high precision.

2) 3.2.2 Reduced Frequency

The reduced frequency is used to express the unsteady nature of flow on airfoils and wings [46]. This parameter is defined as the ratio of the connective timescale ($^{C}/_{U}$) to the forced oscillation timescale ($^{1}/_{\dot{\alpha}}$) [47]. For an airfoil with a length of C, the pitching around one-fourth of the mid-chord at a constant pitching rate, $\dot{\omega}$ (rad/s), the reduced frequency is defined as follows [48].

$$K = \frac{\omega C}{2U} \quad (1)$$

When k=0.1, the connective timescale, and oscillation time scale are of the same order, and the flow is unsteady. Even when the reduced frequency is as low as 0.05, there is a considerable difference between the static and dynamic stall characteristics [53]. According to Leishman, reduced frequencies higher than 0.05 are more critical because the unsteady aerodynamics properties can result in significant fluctuations in the pressure acting on the airfoil or wing surface and increase the lift force. At reduced frequencies lower than 0.05, the flow functions as a quasi-steady flow [50].

Numerous studies have been conducted to understand the effects of reduced frequency on the dynamic stall characteristics of different airfoils, and it has been reported that with an increase in the reduced frequency, the dynamic stall is delayed and transferred to larger attack angles. In addition, the lift force generated by the airfoil cause thrusting and forward movements of air vehicles during flapping.

II. RESULTS AND DISCUSSION

A. 4.1. Aerodynamic Coefficients in the Static State

In our numerical simulations, the NACA 0012 mid-chord length was 1 meter, the flow density was 1000 kg/m3, and the flow Reynolds number was 1100. The numerical analysis of angular airfoil oscillations was carried out in the 3.183-6.3660 frequency range, the 10-20 reduced frequency range, and at the 5-degree average attack angle. The results of the aerodynamic coefficients of the problem solution are presented in the following. The parameters required for solving this problem are listed in Table.1. Since the average attack angle (=5 degrees) and the frequency are known the real-time attack angles are obtained using the following relation.

$$\theta = \theta_0 \sin[2\pi f(t - t_o)] \quad (2)$$

After obtaining the time values and drag coefficient from the problem solution, it is possible to produce the attack angle and thrust coefficient diagrams by time step.

Table.1. The Parameters Required for Solving the Problem in the Angular Oscillation State

Variable	Value
Time step	**0.0015**
Reynolds number	**1100**
Density	**1000 kg/m3**
Viscosity	**0.001**
Length	**1 m**

In any case, the thrust coefficient is obtained from the drag coefficient, and the average thrust is obtained by averaging the thrust coefficients. However, for any K value (i.e., the reduced frequency) one thrust coefficient is obtained. Several examples of the angular oscillation diagrams are depicted in the following. Fig.5, Fig.6, Fig.7, and Fig.8 describe the thrust coefficient variations by time for the k=10, k=14, and k=18 reduced frequencies.

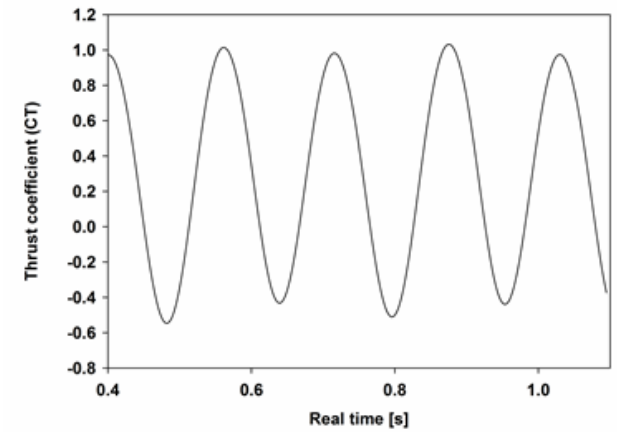

Fig.5. The diagram of thrust coefficient by time in the angular oscillation state for K=10 and f=3.18

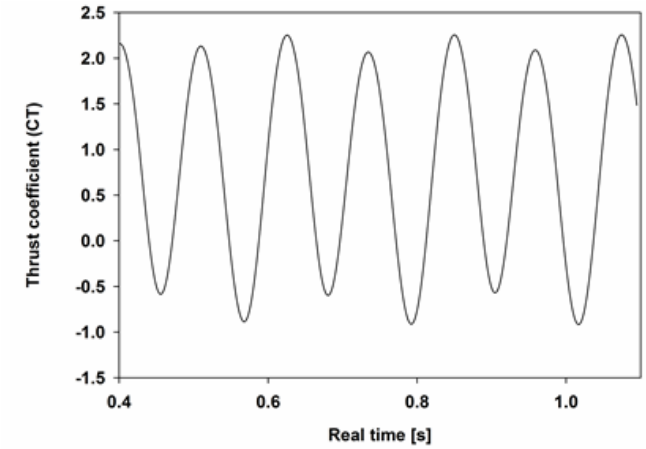

Fig.6. The diagram of thrust coefficient by time in the angular oscillation state for K=14 and f=4.45

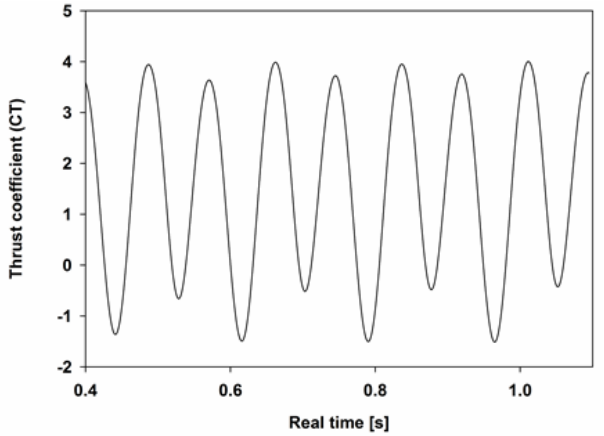

Fig.7. The diagram of thrust coefficient by time in the angular oscillation state for K=18 and f=5.7

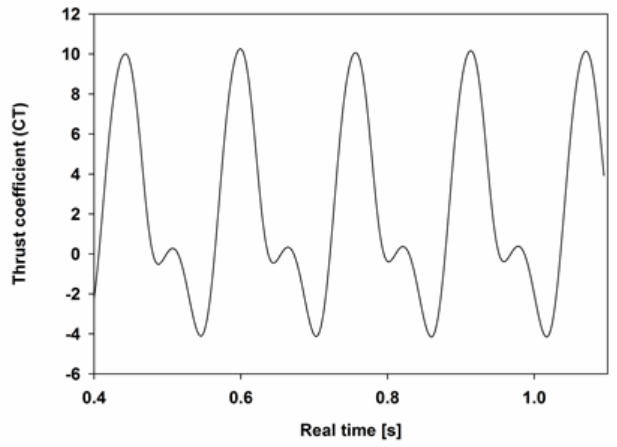

Fig.8. The diagram of thrust coefficient by time in the angular oscillation state for K=20 and f=6.36

As it can be seen in Fig.6, Fig.7 and Fig.8, in the angular oscillation state, if the initial attack angle is invariant and the frequency is variant, with an increase in K the thrust coefficients and the thrust oscillation range increase (i.e., move toward the positive side of the range). The increase in K also results in an increment in the thrust coefficient oscillations.

In an oscillation period at the -0-attack angle (an attack angle close to zero), the thrust decreases to the zero-attack angle and as the attack angle grows, the thrust coefficient increases. As soon as the stall occurs and the attack angles reduces to the As soon as the stall occurs, as the attack angle reduces to the lowest level (a decrease in the negative direction), the lift escalates and then it decreases following the stall. The non-uniform variations of thrust may be caused by the formation of eddies transferred from the leading edge to the wing. The eddy resulted from the separation bubble and its combination with the trailing edge eddy (that is transferred from beneath the wing to the wing surface can disrupt the uniform thrust variations. Thrust increases with an increase in the strength of this combination. To validate the airfoil thrust coefficient in the angular oscillation state, the thrust coefficient is obtained using the drag coefficient in each state, and after averaging the thrust coefficients, one average thrust is obtained for each reduced frequency. Fig.9 shows the thrust coefficient of the problem numerical solution. The airfoil thrust coefficient curve in the angular oscillation state obtained from Fluent was compared to the thrust coefficient curve presented in [2] to validate the results. As seen, there is a slight difference between the results that reflect the satisfactory consistency of these values. As seen in Fig.10, as the reduced frequency grows, the thrust coefficient escalates. The increase in the thrust coefficient is intensified at reduced frequencies higher than 10.

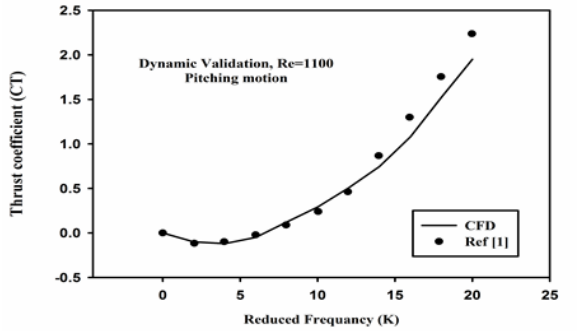

Figure.9. Comparing the variations of the thrust coefficients resulted from our numerical simulation and reference [4]

B. 4.2. Flapping State Results

This simulation was carried out using an unorganized dynamic mesh in which oscillation was caused by coding in Fluent. The parameters required for solving the problem in simulating the flapping oscillation are listed in Table.2.

Table.2. The Parameters Required for Solving the Problem in the Flapping Oscillation State

Variable	Value
Time step	0.001
Reynolds number	1100
Density	1000 kg/m3

zero angle, the thrust declines and then increases to reach the lowest attack angle (i.e., the attack angle decreases along the negative direction). Following stall point, the thrust decreases again.

In an oscillation period at the zero-attack angle, if the lift coefficient is positive, with an increase in the attack angle (an increase in the attack angle along the positive direction) the lift declines.

Viscosity	0.001
Airfoil mid chord length	1 m

In simulating the dynamic flapping motion, the upward and downward motions, which constitute plunging, are modeled using relation (3), and the airfoil pitching motion is simulated using equation.2.

$$h = h_0 \sin[2\pi f(t - t_o) + \Psi] \quad (3)$$

The numerical analysis of the airfoil oscillations in the flapping state was carried out in the 0.05-0.15 frequency range; the 0.1571-0.471 reduced frequency range, and the -12.5-13.30-average attack angle range. The phase difference was 90 degrees and the Strouhal number varied from 0.1 to 3. The aerodynamic coefficients resulted from solving the problem in the flapping oscillation state with the 0.001-time step are shown in Fig.12 and Fig.13. Fig.11 shows the pitching moment coefficient resulted from airfoil flapping in the F1 state, which is a combination of angular oscillation and perpendicular oscillation. The initial time values are omitted (from zero to 1.0) to show the fully periodic oscillations.

Table.3. The Simulation Parameters for Angular and Perpendicular Airfoil Oscillations

f(Hz)	h0/c	Θ0(°)	Ψ0	k	St	α0(°)
0/05	1	30	90	0/157	0/1	-12/56
0/1	1	30	90	0/314	0/2	2/14
0/15	1	30	90	0/471	0/3	13/30
0/2	1	30	90	0/628	0/4	21/49
0/25	1	30	90	0/785	0/5	27/52
0/3	1	30	90	0/942	0/6	32/05
0/35	1	30	90	1/099	0/7	35/55

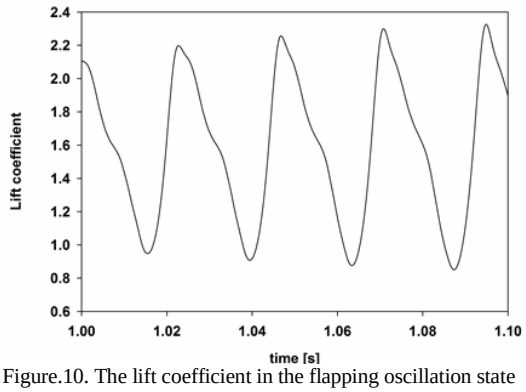

Figure.10. The lift coefficient in the flapping oscillation state

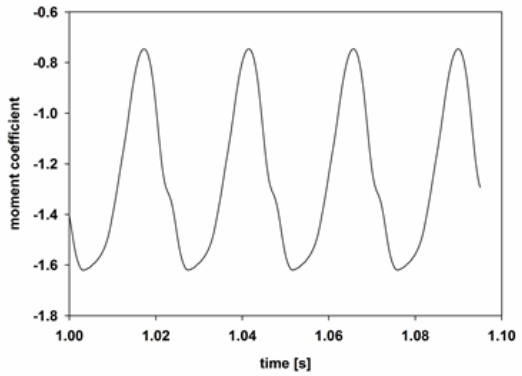

Figure.11. The moment coefficient in the flapping oscillation state

As it can be seen in Fig.12, the thrust coefficient in the flapping oscillation state is varying and the thrust is a forward thrust.

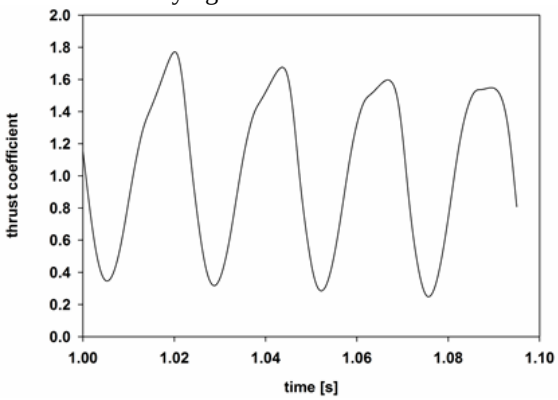

Figure.12. The thrust coefficient in the flapping oscillation state

Fig.13 presents the diagram of the thrust coefficient at the 0.78 reduced coefficient, the 27.5 average attack angle, and the 90-degree phase difference with a Strouhal number of 0.5.

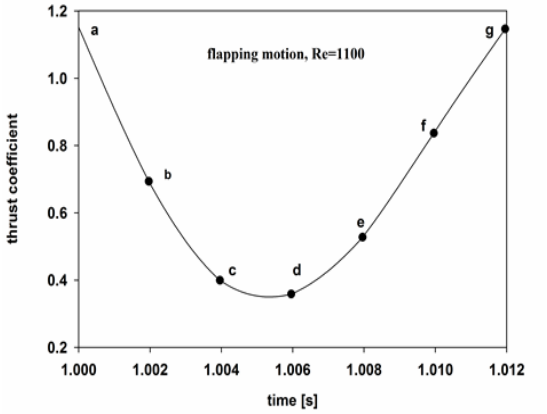

Figure.13. The diagram of thrust coefficient at a single frequency in the flapping state with an attack angle of 27.52 degrees

The contours of the static pressure during airfoil oscillation in the flapping state at the 0.78 reduced frequency are illustrated in Fig.14. In the flapping oscillation, which is a combination of angular and perpendicular oscillations, the increase in the reduced frequency is followed by an increase in the thrust coefficient by the Strouhal number. The highest thrust occurs at the lowest and highest attack angles, and the hrust at the zero-attack angle is almost zero. As seen, with an increase in the reduced frequency, the thrust coefficient oscillation is unsteady. The static stall occurs at the maximum lift coefficient point. At lower values of reduced frequency, the dynamic stall occurs when the attack angle exceeds the static stall attack angle.

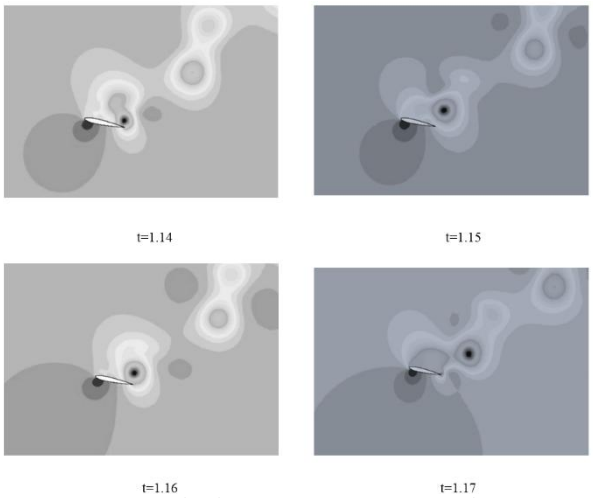

Figure.14. The contours of airfoil oscillation pressure in the flapping state at the 27.52 attack angle

The airfoil aerodynamic coefficients were studied as the reduced frequency remains unchanged and the attack angle changes 0 -12.56, -5, 5, 10, and 15 degrees. Simulation results suggest that the thrust coefficient did not change significantly and in the symmetric attack angle state, the area beneath the diagram of the counter clockwise area of the hysteresis ring becomes symmetrical. Investigation results also indicated that with an increase in the attack angle, the direction of the hysteresis ring of the thrust coefficient changes from the clockwise direction to the counterclockwise direction. However, the clockwise direction of the hysteresis ring of the drag coefficient remains unchanged.

By comparing the airfoil thrust coefficient in the flapping oscillation state in the fluent software to the thrust coefficient in [1], it was found that the result was acceptable and valid.

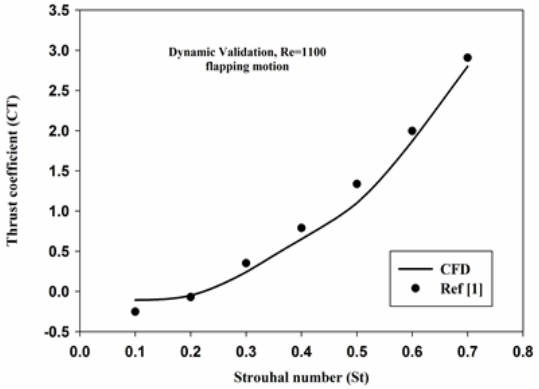

Figure.15. The attack angle by time in the flapping oscillation state

CONCLUSION

The aerodynamic characteristics of a NACA 0012 two-dimensional symmetric airfoil in the perpendicular and angular oscillation states, and the flapping oscillation state, which is a combination of the angular and perpendicular oscillation states, were analyzed numerically in Fluent at different angles. To study the problem, the flow around the airfoil was assumed to be a viscous unsteady flow, and the aerodynamic coefficients were obtained in the static and dynamic states. Research results revealed that with an increase in the reduced frequency, the average thrust coefficient increases. The slope of the increase in the thrust coefficient exceeds ten at larger decreasing frequencies. Moreover, if k>10, the leading-edge eddy that is transferred to the airfoil surface becomes stronger and increases thrust in the ornithopter full cycle. This increase is depicted as a real-time thrust increase in the diagrams, which shows the unsteadiness of the flow at these frequencies. In the flapping oscillation state, the phase difference between the angular oscillation and the vertical oscillation is highly effective, and by adjusting this difference at any reduced frequency, it is possible to obtain the maximum thrust coefficient.

REFERENCE

[1] Soheil Mohtaram, Mohammad Amin Nikbakht, Detect Tool Breakage by Using Combination Neural Decision System & Anfis Tool Wear Predictor, International Journal of Mechanical Engineering and Applications. Vol. 1, No. 2, 2013, pp. 59-63.

[2] Staelens, Y.D., R.F. Blackwelder, and M.A. Page. Novel Pitch Control Effectors for a Blended Wing Body Airplane in Takeoff and Landing Configuration. in 45th AIAA Aerospace Sciences Meeting and Exhibit 8-11 January 2007, Reno, Nevada. AIAA 2007-68.

[3] Abas MFB, Rafie ASBM, Yusoff HB, et al. Flapping wing micro-aerial-vehicle: Kinematics, membranes, and flapping mechanisms of ornithopter and insect flight[J]. Chinese Journal of Aeronautics, 2016, 29(5) : 1159-1177.

[4] McLain, B.K., steady and unsteady aerodynamic flow studies over a 1303 ucav configuration. September 2009, naval postgraduate school.

[5] A. Gilliot , S.M., et al. Static and Dynamic SACCON PIV tests , Part I: Forward Flowfield. in 28th AIAA Applied Aerodynamics Conference 28 June-1 July 2010, Chicago, Illinois. AIAA 2010-4395.

[6] Sirohi, Jayant. "Chapter 5 - Bioinspired and Biomimetic Microflyers." Engineered Biomimicry (2013): 107-138.

[7] Robert, K., et al. Static and Dynamic SACCON PIV Tests, Part II: Aft Flow Field. in 28th AIAA Applied Aerodynamics Conference 28 June-1 July 2010, Chicago, Illinois. AIAA 2010-4396.

[8] Robert, C.N. and P. Alain, The unsteady aerodynamics of slender wings and aircraft undergoing large amplitude maneuvers. Aerospace Sciences, 2003: p. 185–248.

[9] Filippone A. Flight Performance of Fixed and Rotary Wing Aircraft[J]. 2006.

[10] Schutte, A., D. Hummel, and S. M. Hitzel. Numerical and experimental analyses of the vortical flow around the SACCON configuration. in 28th AIAA Applied Aerodynamics Conference 28 June-1 July 2010, Chicago, Illinois. AIAA 2010-4690.

[11] Jani JM, Leary M, Subic A, et al. A review of shape memory alloy research, applications and opportunities[J]. Materials & Design, 2014, 56(4):1078-1113.

[12] Gursula, I., R. Gordnierb, and M. Visbal, Unsteady aerodynamics of nonslender delta wings. Aerospace Sciences, 2005. 41: p. 515–557.

[13] Steven, D.R. and S.A. Andrew, An Inviscid Model for Evaluating Wing Rock Suppression Methodologies, in 32nd Aerospace Sciences Meeting & Exhibit January,Reno. AIAA 94-0808, 1994.

[14] Kramer, M., Increase in the maximum lift of an airfoil due to a sudden increase in its effective angle of attack resulting from a gust. NASA TM-678, 1932.

[15] Harris, F.D. and R.R. Pruyn, Blade Stall Half Fact, Half Fiction. J. Am. Helicopter Soc.13, (1968) 27–48.

[16] Ham, N.D. and M.S. Garelick, Dynamic stall considerations in helicopter rotors. J.Am. Helicopter Soc. 13, (1968) 49–55.

[17] Choudhry, A., M. Arjomandi, and R. Kelso, Horizontal axis wind turbine dynamic stall predictions based on wind speed and direction variability. Mech. Eng., Part A: J. Power Energy 227, (2013) 338–351.

[18] Ferreira, C.S., G.v.B. G. van Kuik, and F. Scarano, Visualization by PIV of dynamic stall on a vertical axis wind turbine. Exp. Fluids 46 (2009) 97–108.

[19] Schreck, S. and M. Robinson, Blade three-dimensional dynamic stall response to wind turbine operating condition. J. Sol. Energy Eng. 127, (2005) 488.

[20] Schreck, S., et al., HAWT dynamic stall response asymmetries under yawed flow conditions. Wind Energy 3, (2000) 215–232.

[21] Shipley, D.E., et al., Evidence that aerodynamic effects, including dynamic stall,dictate HAWT structural loads and power generation in highly transient time frames, in National Renewable Energy Lab,. 1994: United States.

[22] Shipley, D.E., M.S. Miller, and M.C. Robinson, Dynamic stall occurrence on a horizontal axis wind turbine blade, in National Renewable Energy Lab. 1995: United States.

[23] Carr, L.W., Progress in analysis and prediction of dynamic stall, . J. Aircr.25, (1988) 6–17.

[24] Ekaterinaris, J.A. and M.F. Platzer, Computational prediction of airfoil dynamic stall. Aerosp. Sci. 33 (1998) 759–846.

[25] Kerho, M.F., Adaptive airfoil dynamic stall control. J. Aircr. 44 (2007) p. 1350–1360.

[26] Krzysiak, A., Improvement of helicopter performance using self-supplying air jet vortex generators. J. KONES Powertrain Transp, (2013) 20.

[27] Leishman, J. and T. Beddoes, A semi-empirical model for dynamic stall,. J. Am.Helicopter Soc. 34, (1989): p. 3–17.

[28] McCroskey, W., The Phenomenon of Dynamic Stall. DTIC Document, 1981.

[29] McCroskey, W.J., Unsteady airfoils. (1982) Annu. Rev. Fluid Mech. 14. p. 285–311.

[30] Liu, H. and K. Kawachi, A numerical study of insect flight. J. Comput. Phys. 146, (1998) 124–156.

[31] Wang, Z.J., Vortex shedding and frequency selection in flapping flight. J. Fluid Mech. 410 (2000) p. 323–341.

[32] Gheisari, R., et al. "Experimental studies on the ultra-precision finishing of cylindrical surfaces using magnetorheological finishing process." Production & Manufacturing Research 2.1 (2014): 550-557.

[33] Shyy, W., et al., Aerodynamics of Low Reynolds Number Flyers. Cambridge University Press, 2007.

[34] Norberg, U.M.L., Structure, form, and function of flight in engineering and the living world. J. Morphol. 252, (2002) p. 52–81.

[35] Lang, J.D. and M.S. Francis, Unsteady Aerodynamics and Dynamic Aircraft Maneuverability. DTIC Document, 1985.

[36] Niu, Y.-Y. and C.-C. Chang, How do aerodynamic forces of the pitching rigid and flexible airfoils evolve? AIAA J, (2013) p. 1–7.

[37] Visbal, M.R., Dynamic stall of a constant-rate pitching airfoil. J. Aircr. 27 (1990): p. 400–407.

[38] Karim, M.A. and A. Mukund, Suppression of Dynamic-Stall Vortices over Pitching Airfoils by Leading-Edge Suction. AIAA, August 1994. 32.

[39] Lars, E.E. and J.P. Reding, Dynamic Stall at High Frequency and Large Amplitude. J. AIRCRAFT. 17: p. 136-142.

[40] Francis, M.S. and J.E. Keesee, Airfoil Dynamic Stall Performance with Large-Amplitude Motions. AIAA. 23.

[41] Lawrence, W.C., Progress in Analysis and Prediction of Dynamic Stall. AIRCRAFT, january 1988. 25: p. 6-17

[42] Mohtaram, Soheil, et al. "Energy-exergy analysis of compressor pressure ratio effects on thermodynamic performance of ammonia water combined cycle." Energy Conversion & Management 134(2017):77-87.

[43] Mohtaram, Soheil, et al. "Evaluating the effect of ammonia-water dilution pressure and its density on thermodynamic performance of combined cycles by the energy-exergy analysis approach." Mechanics 23.2 (2017): 209-219.

[44] Anderson, J.D., Fundamentals of Aerodynamics. 2001., New York: McGraw-Hill.

[45] Leishman, J., Dynamic stall experiments on the NACA 23012 aerofoil. Exp.Fluids 9, 1990: p. 49–58.

[46] Gupta, S. and J.G. Leishman, Dynamic stall modelling of the S809 aerofoil and comparison with experiments. Wind Energy 9, (2006): p. 521–547.

[47] Digavalli, S.K., Dynamic Stall of a NACA 0012 Airfoil in Laminar Flow. 1994., Massachusetts Institute of Technology.

[48] Jumper, E., S. Schreck, and R. Dimmick, Lift-curve characteristics for an airfoil pitching at constant rate. J. Aircr. 24, (1987) p. 680–687.

[49] Ramsay, R.R., M.J. Hoffmann, and G.M. Gregorek, Effects of Grit Roughness and Pitch Oscillations on the S809 Airfoil. NREL/TP-442-7817, National Renewable Energy Laboratory, 1995.

[50] Leishman, J.G., Principles of Helicopter Aerodynamics. 2006.: Cambridge University Press.

[51] Rival, D. and C. Tropea, Characteristics of pitching and plunging airfoils under dynamic-stall conditions. J. Aircr. 47, (2010): p. 80–86.

[52] S.J. Schreck, Unsteady Vortex Dynamics and Surface Pressure Topologies on a Finite Pitching Wing. 1994., DTIC Document

Nomenclature:

L	Length	l	Characteristic length
Cf	Force coefficient	P	Static pressure
CD	Drag coefficient	Re	Reynolds number
CL	Lift coefficient	St	Strouhal number
Cm	Moment coefficient	A	Angle of attack
F	Flapping coefficient	M	Dynamic viscosity coefficient
G	Gravity acceleration	ρ	Fluid density
t	Time	θ	Angle
f	frequency	θ0	Initial angle
ω	Angular velocity	h	Displacement height
k	Reduced frequency	h0	Initial displacement height
		Ψ	Initial phase